Nucleolin is a nuclear target of heparan sulfate derived from glypican-1

Cheng, Fang; Belting, Mattias; Fransson, Lars Åke; Mani, Katrin

Published in:
Experimental Cell Research

DOI:
10.1016/j.yexcr.2017.03.021

2017

Document Version:
Peer reviewed version (aka post-print)

Nucleolin is a nuclear target of heparan sulfate derived from glypican-1

Fang Cheng[a], Mattias Belting[b], Lars-Åke Fransson[a], and Katrin Mani[a,*]

[a] Department of Experimental Medical Science, Division of Neuroscience, Glycobiology Group, Lund University, Biomedical Center A13, SE-221 84, Lund, Sweden.

[b] Department of Clinical Sciences, Section of Oncology and Pathology, Lund University, Lund, Sweden

[*]Address correspondence to Katrin Mani, katrin.mani@med.lu.se

Keywords: Anhydromannose; Glypican; Heparan sulfate; Histones; Nucleolin; RNA

Abstract

The recycling, S-nitrosylated heparan sulfate (HS) proteoglycan glypican-1 releases anhydromannose (anMan)-containing HS chains by a nitrosothiol-catalyzed cleavage in endosomes that can be constitutive or induced by ascorbate. The HS-anMan chains are then transported to the nucleus. A specific nuclear target for HS-anMan has not been identified. We have monitored endosome-to-nucleus trafficking of HS-anMan by deconvolution and confocal immunofluorescence microscopy using an anMan-specific monoclonal antibody in non-growing, ascorbate-treated, and growing, untreated, wild-type mouse embryonic fibroblasts and hypoxia-exposed Alzheimer mouse Tg2576 fibroblasts and human U87 glioblastoma cells. In all cells, nuclear HS-anMan targeted a limited number of sites of variable size where it colocalized with DNA and nucleolin, an established marker for nucleoli. HS-anMan also colocalized with ethynyl uridine-tagged nascent RNA and two acetylated forms of histone H3. Acute hypoxia increased the formation of HS-anMan in both Tg2576 and U87 cells. A portion of HS-anMan colocalized with nucleolin at small discrete sites, while most of the nucleolin and nascent RNA was dispersed. In U87 cells, HS-anMan, nucleolin and nascent RNA reassembled after prolonged hypoxia. Nucleolar HS may modulate synthesis and/or release of rRNA.

Introduction

Glypicans (Gpc) are a family of cell-surface heparan sulfate (HS) proteoglycans that regulate growth-factor and morphogen signaling [1, 2]. The Gpc-1 protein, which is ubiquitously expressed in vertebrate tissues, consists of a large N-terminal α-helical domain containing 14 conserved, disulfide-bonded Cys residues followed by a flexible HS-attachment region and the C-terminal glycosylphosphatidylinositol membrane anchor [3] as shown in Fig. 1A. The flexible region also contains two non-conserved Cys residues that are not disulfide bonded (Cys-SH) and can be S-nitrosylated (Cys-SNO) in a copper-dependent reaction [4, 5]. *In vitro,* the SNO groups in recombinant Gpc-1 can catalyze deaminative cleavage of the HS chains at N-unsubstituted glucosamines in a reaction that is induced by ascorbate. This results in the release of HS chains and oligosaccharides containing reducing terminal anhydromannose (HS-anMan) and a Gpc-1 core protein with short HS stubs as shown in Fig. 1B.

In cell cultures, cell surface Gpc-1 is internalized via a caveolin-1-associated pathway, S-nitrosylated and transported to endosomes where the SNO/nitric oxide (NO)-catalyzed autodegradation takes place. Formation of HS-anMan is constitutive in dividing fibroblasts and suppressed in non-dividing ones but can be restored by exogenously supplied ascorbate [6, 7].

HS as well as other glycosaminoglycans have been found in various cell nuclei [8-11]. It is not known how HS is transported to the nucleus, nor if it is associated with specific nuclear structures. We have recently shown, by immunofluorescence microscopy using an anMan-specific monoclonal antibody and by [^{35}S]sulfate-labeling and isolation of nuclear HS, that HS-anMan generated by ascorbate treatment of wild-type mouse embryonic fibroblasts (WT MEF) and N2a neuroblastoma cells penetrates the endosomal membrane and translocates

to the nucleus. Penetration and transfer was dependent on expression and processing of the amyloid precursor protein. HS-anMan eventually disappeared from the nucleus and was captured in autophagosomes/lysosomes for final destruction [12]. Here, we show that nucleolin is involved in nuclear targeting of HS-anMan suggesting that HS-anMan interacts with nucleoli.

Materials and Methods

Cells and reagents

Mouse embryonic fibroblasts (MEF) from wild-type (WT) mice and the Alzheimer mouse model Tg2576 were the same as described previously [13, 14]. Human U87 MG cells established from a glioblastoma multiforme tumour were obtained from ATCC. The vector used for silencing of mouse Gpc-1 was the same as described previously [14]. Actinomycin D was purchased from Fisher scientific. The DNA staining compound 4,6-diaminido-2-phenylindole (DAPI) and ascorbic acid were from Sigma-Aldrich. The monoclonal antibody against anhydromannose (mAb AM) was originally described by Pejler *et al.* [15] and previously used in several studies from this laboratory [5, 6, 12-14]. The polyclonal antibodies were: anti-mouse Gpc-1 [14], anti-nucleolin (NCL, ab22758, Abcam), anti-histone H3 with N-acetylated N-terminal (H3NAc, 06-755, Millipore), anti-histone H3 with acetylated Lys-9 (H3K9, ab10812, Abcam), and anti-histone H3 with dimethylated Lys-9 ($H3K9Me_2$, ab194680, Abcam). FITC-labeled goat anti-mouse Ig was from Sigma and Alexa-Fluor 594-labeled donkey anti-rabbit IgG from Life Technologies.

Cell culture, transfection and nascent rRNA detection

Cells were grown in minimal essential medium containing glutamine, penicillin, streptomycin and 10% fetal bovine serum in 1-cm^2 micro-culture plates at a seeding density of 10,000-20,000 cells/well and then grown to near confluence. Cells seeded at a density of 10,000/cm^2 were grown for 24 h, growth-arrested in 0.2% serum for 48 h and then grown in 10% serum for various periods of time. Experiments were performed with cultures either kept under normoxic (21% O_2) conditions or exposed to hypoxia (1% O_2) in an InVivo$_2$ Hypoxia Work Station 400 (Ruskinn Technology Ltd) for various periods of time. Transfections were performed as described earlier (14).

For pulse labelling of RNA, cells were incubated for 30 min with 1 mM 5-ethynyl uridine and fixed with 4% paraformaldehyde/PBS. Labeled transcripts were detected using Alexa Fluor 594 azide (Click-it RNA imaging Kit, Thermo Fisher Scientific). Total RNA was isolated using the RNeasy Mini Kit (Qiagen 74104) and rRNA was recovered using the Ribo-Zero Magnetic Kit (Illumina) according to the manufacturer´s protocols and quantified by UV-absorbance.

Immunofluorescence microscopy

Cells were examined by deconvolution or confocal laser immunofluorescence microscopy as described previously (12). In brief, cells were fixed in acetone or paraformaldehyde/PBS (for RNA detection) in order to retain cellular and subcellular structures and to ensure the preservation of carbohydrates. The fixed cells were first pre-coated with 10% anti-mouse total Ig and then exposed to primary antibodies overnight. The secondary antibodies used were FITC-tagged goat antimouse Ig when the primary antibody was a monoclonal and Alexa Fluor

594-tagged goat anti-rabbit IgG or sometimes Alexa Fluor 594-tagged donkey anti-goat IgG when the primary antibody was a polyclonal. In the controls, the primary antibody was omitted. DNA staining with 4,6-diamidino-2-phenylindole (DAPI), as well as staining with antibodies was performed as recommended by the manufacturers. The fluorescent images were analyzed by using a Carl Zeiss AxioObserver inverted fluorescence microscope with deconvolution technique and equipped with objective EC “Plan-Neofluar” 63x/ 1.25 Oil M27 and AxioCam MRm Rev Camera. Identical exposure settings and times were used for all images. During microscopy, the entire slides were scanned and representative immunofluorescence images containing many cells were captured. To determine the fluorescence intensity AxioVision 4 modul IntMeasure was used to automatically calculate the intensities of the same sized area in each image. Images were also taken using the Z-stacking function in the AxioVision Release 4.8 software. Fluorophores were excited in a sequential manner using multitrack acquisition to minimize channel cross-talk. Confocal laser immunofluorescence microscopy was performed using a Zeiss LSM 710 laser scanning microscope with a C-apochromat 63X/1.20 water correction ring objective and Zen 2009 software.

Results

HS-anMan released from Gpc-1 in ascorbate-treated, near confluent WT MEF preferentially targets nucleolin

To confirm that HS-anMan is derived from Gpc-1 in WT-MEF we suppressed Gpc-1 expression using siRNA (Fig. S1A, C). This resulted in a corresponding decrease of ascorbate-induced HS-anMan staining indicating that Gpc-1 is a precursor of HS-anMan (Fig.

S1B, D). We previously observed that nuclear HS-anMan staining was unevenly distributed and was preferentially associated with certain sites [12]. Nucleolin is a characteristic component of nucleoli [for a recent review, see 16]. Staining for nucleolin appeared most strongly at a limited number sites in the nuclei of untreated near confluent WT MEF (Fig. 2A, t=0, red). HS-anMan staining, which was initially nearly undetectable (Fig. 2A, t=0, green), was induced by ascorbate at cytoplasmic sites (Fig. 2A, t=7 min, green) and then HS-anMan was imported into the nuclei (Fig 2A, t=10-15 min, green). Colocalization of HS-anMan with nucleolin was seen after 15 min (Fig. 2A, t=15 min, yellow) and confirmed by top to bottom sectioning of cell nuclei which were analyzed both by deconvolution (Fig. 2B, yellow) and by confocal immunofluorescence microscopy (Fig. 2C, yellow).

We previously observed that, during chase in fresh medium, HS-anMan disappeared from the nucleus and was captured in autophagosomes [12]. As shown here, a portion remained for up to 24 h (Fig. 3A-D, AM) and was concentrated to sites where it colocalized with DNA (Fig. 3C and 3D, AM/DAPI, turquoise dots). During chase, nucleolin staining became slightly dispersed (Fig. 3E-H, NCL) and the remaining HS-anMan colocalized only partly with nucleolin (Fig. 3G and 3H, NCL/AM, yellow).

Nucleolin that is associated with nucleoli has a slow turn-over. Depletion of nuclear nucleolin has been obtained by inhibition of transcription with actinomycin D [17]. We treated near confluent cultures of WT-MEF with actinomycin D followed by ascorbate to induce HS-anMan formation. In untreated cells, where staining for HS-anMan was almost undetectable (Fig. 4A, AM), nucleolin staining was mostly concentrated to a limited number of sites in the nuclei (Fig. 4A, NCL). Treatment with 5 μg/ml of actinomycin D for 5 h had no effect on nucleolin staining in the nuclei (Fig. 4B, NCL). After treatment with 10 μg/ml actinomycin D for 5 h, there was very little nucleolin staining in the nuclei and weak staining in the cytoplasm (Fig. 4C, NCL). Induction of HS-anMan formation by ascorbate after

treatment with actinomycin D (see arrows in Fig. 4) indicated that when nucleolin was present in the nucleus (Fig. 4D, NCL), HS-anMan was transported to the nucleus (Fig. 4D, AM and AM/NCL, yellow), but when nucleolin was absent from the nucleus (Fig. 4E, NCL), HS-anMan remained in the cytoplasm (Fig. 4E, AM).

HS-anMan released from Gpc-1 in ascorbate-treated, near confluent WT MEF associates with rRNA and acetylated histone H3

The nucleolus is the site of rRNA synthesis. Nascent total RNA synthesis was visualized by incubating near confluent WT MEF with ethynyl uridine followed by coupling to Alexa Fluor 594 azide. In untreated cells, patches of strong nascent RNA staining were observed against a background of weaker staining (Fig. 5A, RNA). The patches of nascent RNA appeared to increase in intensity upon ascorbate treatment and rRNA took up a greater proportion of total RNA (Fig. 5B, RNA and inset). Ascorbate-induced, nuclear HS-anMan staining colocalized with these RNA patches (Fig. 5B, and 5C AM/RNA, yellow). In the center of these patches we frequently observed black holes (see arrows). It is known that when cells are stained for DNA or nascent RNA, nucleoli appear as dark holes, presumably because the nucleolus-associated chromatin is densely packed and partly inaccessible to the various reagents [18, 19]. During chase, part of the HS-anMan staining remained in the holes located near the RNA patches (Fig. 5D, AM, green dots, see arrows).

HS is a polyanion that can bind to the positively charged histones and thereby interfere with histone modifications. Ascorbate-induced, nuclear HS-anMan colocalized with N-terminally acetylated histone H3 (Fig. 6B, AM/N-Ac-H3, yellow). During chase, the remaining HS-anMan staining appeared separately in the holes surrounded by a ring of HS-anMan colocalizing with N-terminally acetylated histone H3 (Fig. 6C-E, AM/N-Ac-H3,

yellow). Similar results were obtained when an antibody against histone H3 with acetylated Lys-9 was applied (Fig. 6F, AM/H3K9Ac, yellow). Colocalization between HS-anMan and histone H3 with dimethylated Lys-9 appeared somewhat weaker (Fig. 6G, AM/H3K9Me_2). Hence, HS-anMan appears to associate primarily with acetylated forms of nucleolar histone H3.

HS-anMan spontaneously generated in growing WT-MEF associates with nucleolin and rRNA

In growing WT-MEF, HS-anMan is spontaneously generated by an unknown mechanism [6, 7]. To examine nuclear targeting of HS-anMan, sparse cultures of WT MEF were growth-arrested by serum deprivation. Growth was then initiated by addition of serum. HS-anMan staining was observed throughout the growth-phase (Fig. 7A-C, AM) and it was present both in the cytoplasm and in the nucleus, where it colocalized with nucleolin (Fig. 7A-C, AM/NCL, yellow). There was also colocalization between nuclear HS-anMan and nascent RNA (Fig. 8A-C, AM/RNA, yellow). Thus, also spontaneously generated HS-anMan was transported to the nucleus and appeared to target the nucleoli.

Effect of hypoxia-induced nuclear HS-anMan on nucleolin and rRNA in Tg2576-MEF and U87 glioblastoma cells

Non-growing MEFs derived from the Alzheimer mouse Tg2576 generate HS-anMan due to a stress-activated generation of NO from endogenous nitrite, which is greatly enhanced by hypoxia [14, 20, 21]. Under normoxic conditions, when nucleolin staining appeared at a limited number of sites in the nuclei (Fig. 9A, NCL), the HS-anMan staining was mainly extranuclear

(Fig. 9A, AM and AM/NCL). After 2 h of hypoxia, there was an increased staining for HS-anMan (Fig. 9B, AM). A portion of the HS-anMan staining appeared at small discrete sites in the nuclei, whereas nucleolin staining was dispersed and filled the nuclei, except for a few empty sites (Fig. 9B, NCL). Colocalization between HS-anMan and nucleolin appeared at small diverse loci in the nuclei between the empty sites (Fig. 9B, AM/NCL, yellow).

Under normoxic conditions, staining for nascent RNA appeared near the dark holes in the nuclei but also elsewhere in the nucleoplasm (Fig. 9C, red). After 2 h of hypoxia staining for nascent RNA and nuclear HS-anMan colocalized also near the nuclear membrane (Fig 9D, AM/RNA).

Cancer cells constitutively generate HS-anMan [6]. In this study we used human U87 glioblastoma cells. Also in these cells, most of the HS-anMan staining was extranuclear (Fig. 10A, AM), but nuclear HS-anMan staining colocalized with nucleolin (Fig. 10A, AM/NCL, orange). Glioma cells respond to hypoxia in many ways including an increased NO formation [22]. Acute hypoxia (30 min) induced an increased HS-anMan staining both in the cytoplasm and in the nucleus of U87 glioblastoma cells (Fig. 10B, AM). At later time-points (2 h and 24 h), nuclear HS-anMan staining became concentrated to a few large sites (Fig. 10C and 10D, AM). After 30 min of hypoxia, nucleolin staining filled the nuclei, except for a few empty sites (Fig. 10B, NCL). At later time-points (2 h and 24 h), nucleolin staining became more concentrated to a few sites, where it colocalized with HS-anMan (Fig. 10C and 10D, AM/NCL, yellow).

Under normoxic conditions, staining for nascent RNA in U87 cells appeared throughout the nucleus and colocalized partially with nuclear HS-anMan (Fig. 11A, AM/RNA, orange). After 24 h of hypoxia, colocalization between nascent RNA and HS-anMan was heterogeneous, *i.e.* strong in some cells and weaker in others (Fig. 11B, low magnification,

AM/RNA, orange/yellow). Strong colocalization was concentrated to a few, enlarged sites (Fig. 11B, high magnification, AM/RNA, yellow).

Discussion

Previous results have shown that there is an endosome-cytosol-nucleus traffic route for HS-anMan released from Gpc-1 by SNO-catalyzed cleavage in endosomes. Exit from the endosomes is probably guided by amyloid beta or related degradation products [12]. The present results demonstrate that nuclear HS-anMan has an affinity for nucleolin suggesting that nucleoli are a primary target. Nucleolin has a bipartite nuclear localization signal sequence [23] and basic sequences in the C-terminal domain [16] that could bind the negatively charged HS-anMan and carry it to the nucleus.

Earlier studies have implicated histones, transcription factors, kinases and topoisomerases as target molecules for nuclear HS [24, 25 and refs. therein]. All of these are present in nucleoli as well as throughout the nucleoplasm. According to current models, nucleolin associates with transcriptionally active rDNA genes and activates rRNA formation. At active nucleolar genes the histones possess euchromatic marks such as acetylated histone H3 [16 and refs. therein]. The rRNA genes are regulated by various epigenetic modifications of histones H3 and H4. Acetylation/methylation of Lys-9 in histone H3 correlates with nucleolar gene activation/repression [16]. Previous studies have shown that glycosaminoglycans, such as HS or heparin, can inhibit histone acetyl transferase *in vitro* [26]. Suppression of N-terminal acetylation in histone H3 by nuclear glycosaminoglycans in tumor cells has also been observed [27]. HS-anMan colocalized both with nucleolin and with acetylated histone H3, suggesting an involvement in rRNA formation and/or release.

There is over-expression of nucleolin in highly proliferative cells, such as cancer cells, and under stress conditions [16, 28 and refs. therein]. In the latter case, nucleolin redistributes from the nucleolus to the nucleoplasm. Acute hypoxia induced a similar effect in both Tg2576 MEF and U87 glioblastoma cells concomitant with a substantial increase in nuclear HS-anMan. In many cases, separate staining for HS-anMan was conspicuous in the center of the presumed nucleoli, which was devoid of both histone and nascent RNA staining. The epitope for anti-HS-anMan is located at the reducing end of the long linear HS chain, while the non-reducing end often has the highest negative charge density [29]. If the latter HS region interacts with histones in the center of nucleoli and the HS chain extends away from the center, the epitope may be more easily detected. In conclusion, the polyanionic HS can bind to many basic proteins, including histones and nucleolin, and thereby interfere with their interactions with DNA and RNA.

References

1. Häcker U, Nybakken K, Perrimon N. Heparan sulfate proteoglycans. The sweet side of development. Nat Rev Mol Cell Biol. 2005; 6(7):530-41. doi:10.1038/nrm1681
2. Bülow HE, and Hobert O. The molecular diversity of glycosaminoglycans shapes animal development. Annu Rev Cell Dev Biol. 2006; 22:375-407. doi:10.1146/annurev.cellbio.22.010605.093433
3. Svensson G, Awad W, Håkansson M, Mani K, Logan DT. Crystal structure of N-glycosylated human glypican-1 core protein. Structure of two loops evolutionary conserved in vertebrate glypican-1. J Biol Chem. 2012; 287(17):14040-51. doi:10.1074/jbc.M111.322487

4. Svensson G, Mani K. S-nitrosylation of secreted recombinant glypican-1. Glycoconj J. 2009; 26(9):1247-57. doi: 10.1007/s10719-009-9243-z
5. Cheng F, Svensson G, Fransson L-Å, Mani K. Non-conserved, S-nitrosylated cysteines in glypican-1 react with N-unsubstituted glucosamines in heparan sulfate and catalyze deaminative cleavage. Glycobiology. 2012; 22(11):1480-6. Epub 2012 Jul 16. doi: 10.1093/glycob/cws111
6. Mani K, Cheng F, Fransson L-Å. Constitutive and vitamin C-induced, NO-catalyzed release of heparan sulfate from recycling glypican-1 in late endosomes. Glycobiology. 2006; 16(12):1251-61. Epub 2006 Sep 12. doi:10.1093/glycob/cwl045
7. Fransson L-Å, Mani K. Novel aspects of vitamin C: how important is glypican-1 recycling. Trends Mol Med. 2007; 13(4):143-9. Epub 2007 Mar 6. doi:10.1016/j.molmed.2007.02.005
8. Bhavanandan VP, Davidson EA. Mucopolysaccharides associated with nuclei of cultured mammalian cells. Proc Natl Acad Sci U.S.A. 1975; 72(6):2032-6.
9. Fedarko NS, Conrad HE. A unique heparan sulfate in the nuclei of hepatocytes. Structural changes with the growth state of the cells. J Cell Biol. 1986; 102(2):587-99.
10. Ishihara M, Fedarko NS, Conrad HE. Transport of heparan sulfate into the nuclei of hepatocytes. J Biol Chem. 1986; 261(29):13575-80.
11. Hiscock DRR, Yanagishita M, Hascall VC. Nuclear localization of glycosaminoglycans in rat ovarian granulosa cells. J Biol Chem. 1994; 269(6):4539-46.
12. Cheng F, Cappai R, Lidfeldt J, Belting M, Fransson L-Å, Mani K. APP/APLP2 expression is required to initiate endosome-nucleus-autophagosome trafficking of

glypican-1-derived heparan sulfate. J Biol Chem. 2014; 289(30):20871-8. doi:10.1074/jbc.M114.552810

13. Cappai R, Cheng F, Ciccotosto GD, Needham BE, Masters CL, Multhaup G, et al. The amyloid precursor protein (APP) of Alzheimer disease and its paralog, APLP2, modulate the Cu/Zn-nitric oxide-catalyzed degradation of glypican-1 heparan sulfate in vivo. J Biol Chem. 2005; 280(14):13913-20. Epub 2005 Jan 27. doi:10.1074/jbc.M409179200
14. Cheng F, Cappai R, Ciccotosto GD, Svensson G, Multhaup G, Fransson L-Å, et al. Suppression of amyloid β A11 antibody immunoreactivity by vitamin C. Possible role of heparan sulfate oligosaccharides derived from glypican-1 by ascorbate-induced, nitric oxide (NO)-catalyzed degradation. J Biol Chem. 2011; 286(31):27559-72. Epub 2011 Jun 3. doi:10.1074/jbc.M111.243345
15. Pejler G, Lindahl U, Larm O, Scholander E, Sandgren E, Lundblad A. Monoclonal antibodies specific for oligosaccharides prepared by partial nitrous acid deamination of heparin. J Biol Chem. 1988; 263(11):5197-201.
16. Durut N, Sáez-Vásquez J. Nucleolin: Dual roles in rDNA chromatin transcription. Gene. 2015; 556(1):7-12. Epub 2014 Sep 16. doi:10.1016/j.gene.2014.09.023
17. Hovanessian AG, Soundaramourthy C, El Khoury D, Nondier I, Svab J, Krust B. Surface expressed nucleolin is constantly induced in tumor cells to mediate calcium-dependent ligand internalization. PloS ONE, 2010; 5(12):e15787. doi:10.1371/journal.pone.0015787
18. Smirnov E, Cmarko D, Mazel T, Hornácek M, Raska I. Nucleolar DNA: the host and the guests. Histochem Cell Biol. 2016; 145(4):359-72. Epub 2016 Feb 4. doi:10.1007/s00418-016-1407-x

19. Cudron-Herger M, Pankert T, Seiler J, Németh A, Voit R, Grummt I, et al. Alu element-containing RNAs maintain nucleolar structure and function. EMBO J. 2015; 34(22):2758-74. Epub 2015 Oct 13. doi:10.15252/embj.201591458
20. Cheng F, Fransson L-Å, Mani K. Rapid nuclear transit and impaired degradation of amyloid β and glypican-1-derived heparan sulfate in Tg2576 mouse fibroblasts. Glycobiology. 2015; 25(5):548-56. Epub 2014 Dec 19.doi:10.1093/glycob/cwu185
21. Cheng F, Bourseau-Guilmain E, Belting M, Fransson L-Å, Mani K. Hypoxia induces NO-dependent release of heparan sulfate in fibroblasts from the Alzheimer mouse Tg2576 by activation of nitrite reduction. Glycobiology. 2016; 26(6):623-34. Epub 2016 Jan 20. doi:10.1093/glycob/cww007
22. Harris AL. Hypoxia-a key regulatory factor in tumor growth. Nat Rev Cancer. 2002; 2(1):38-47. doi:10.1038/nrc704
23. Tajrishi MM, Tuteja R, Tuteja N. Nucleolin: the most abundant multifunctional phosphoprotein of nucleolus. Commun Integr Biol. 2011; 4(3):267-75. doi:10.4161/cib.4.3.14884
24. Dudas J, Ramadori G, Knittel T, Neubauer K, Raddatz D, Egedy K, et al. Effect of heparin and liver heparan sulphate on interaction of HepG2-derived transcription factors and their cis-acting elements: altered potential of hepatocellular carcinoma heparan sulphate. Biochem J. 2000; 350 Pt 1:245-51.
25. Stewart MD, Sanderson RD. Heparan sulfate in the nucleus and its control of cellular functions. Matrix Biol. 2013; 35:56-9. Epub 2013 Dec 3. doi:10.1016/j.matbio.2013.10.009

26. Buczek-Thomas JA, Hsia E, Rich CB, Foster JA, Nugent MA. Inhibition of histone acetyl transferase by glycosaminoglycans. J Cell Biochem. 2008; 105(1):108-20. doi:10.1002/jcb.21803

27. Nilsson U, Johnsson R, Fransson L-Å, Ellervik U, Mani K. Attenuation of tumor growth by formation of antiproliferative glycosaminoglycans correlate with low acetylation of histone H3. Cancer Res. 2010; 70(9):3771-9. Epub 2010 Apr 20. doi:10.1158/0008-5472.CAN-09-4331

28. Berger CM, Gaume X, Bouvet P. The roles of nucleolin subcellular localization in cancer. Biochimie. 2015; 113:78-85. Epub 2015 Apr 9. doi:10.1016/j.biochi.2015.03.023

29. Lindblom A, Bengtsson-Olivecrona G, Fransson L-Å. Domain structure of endothelial heparan sulphate. Biochem J. 1991; 279 (Pt 3):821-9.

Funding: This work was supported by grants from the Swedish Research Council, the Swedish Cancer Society, Axel Linders, Alfred Österlund, Åhlen, Stohnes, and Olle Engkvist Foundations.

Abbreviations: anMan/AM, anhydromannose; DAPI, 4,6-diamidino-2-phenylindole; Gpc, glypican; HS, heparan sulfate; mAb, monoclonal antibody; MEF, mouse embryonic fibroblast; NO, nitric oxide; SH, thiol; SNO, S-nitrosothiol; Tg2576, transgenic Alzheimer mouse; WT, wild-type.

Figure legends

Fig 1. Structure of the Gpc-1 proteoglycan and the mechanism for SNO/NO-dependent deaminative cleavage of HS. (A) The Gpc-1 core protein consists of a large N-terminal, α-helical, globular domain that contains 7 disulfide bonds (C-C) and two N-linked glycans (GlcNAc), an unstructured stem region to which the polyanionic (----) HS chains (string of green hexagons) are attached and a C-terminus that is anchored to the membrane via a glycolipid (yellow dot). The stem region and the HS chains are not drawn to scale, the latter should extend far beyond the globular N-terminal domain. (B) In addition to the 3 HS chains **(——),** the C-terminal stem region also contains 2 Cys with free thiols/thiolates ($^{-}$S-C). These can be S-nitrosylated by nitrosonium ions (NO^{+}) in a copper-dependent reaction. The HS chains contain clusters of N-unsubstituted glucosamines ($GlcNH_2$/$GlcNH_3^{+}$, only one of which is depicted as a hexagon), preferentially located near the linkage region to the protein core. Attraction between $GlcNH_3^{+}$ and the nitrosothiol dipol ($^{\delta-}ONS^{\delta+}$-C) favors an NO-catalyzed reaction that converts the amino group to a diazonium ion (-N=N^{+}). The diazotized glucosamine undergoes a spontaneous ring contraction accompanied by cleavage of the glycosidic bond releasing HS with a reducing terminal anMan residue (pentagon), exposing C-1 as a free aldehyde (-CHO) and leaving behind a Gpc-1 with truncated HS stubs.

Fig. 2. HS-anMan released from Gpc-1 by ascorbate and transported to the nucleus targets nucleolin. (A) Deconvolution immunofluorescence microscopy images of near confluent WT-MEFs which were either untreated or treated with 1 mM ascorbate for the indicated periods of time. Staining was performed with mAb anti-HS-anMan (AM, green) and anti-nucleolin (NCL, red). Exposure time was the same in all cases. (B) Horizontal top to bottom sections of a deconvolution immunofluorescence microscopy image of cell treated with ascorbate for 13 min. (C) Horizontal top to bottom sections of a confocal laser immunofluorescence

microscopy images of cells treated with ascorbate for 13 min. Distances from the top are indicated below the images.

Fig. 3. Nuclear HS-anMan is retained by nucleolin during chase. Deconvolution immunofluorescence microscopy images of near confluent cultures of WT MEFs which were (A, E) untreated or (B, F) treated with 1 mM ascorbate (Asc) for 30 min followed (C, D, G, H) by chase in fresh medium for the indicated periods of time. Staining was performed with mAb anti-HS-anMan (AM, green), DAPI (DNA, nuclei, blue) and anti-nucleolin (NCL, red). Exposure time was the same in all cases.

Fig. 4. Treatment with actinomycin D prevents ascorbate-induced nuclear transport of HS-anMan. Deconvolution immunofluorescence microscopy images of near confluent cultures of WT MEFs which were (A) untreated or (B, C) treated with actinomycin D at 5 or 10 μg/ml for 5 h followed (D, E) by 1 mM ascorbate for 15 min. Staining was performed with mAb anti-HS-anMan (AM, green) and anti-nucleolin (NCL, red). Exposure time was the same in all cases.

Fig 5. Association between ascorbate-induced nuclear HS-anMan and nascent RNA. Deconvolution immunofluorescence images of near confluent cultures of WT MEFs which were (A) untreated or (B) treated with 1 mM ascorbate (Asc) for 30 min, followed (C, D) by chase in fresh medium for the indicated periods of time. Staining was performed with mAb anti-HS-anMan (AM, green) and nascent RNA was visualized by pulse labeling with ethynyl uridine followed by coupling to Alexa Fluor 594 azide (RNA, red). Exposure time was the same in all cases. Insets in (A-B) show quantification of rRNA by using a magnetic ribosomal RNA probe (average of two measurements). Samples containing equal amounts of total RNA

were analyzed. Arrows in B and C show some of the unstained holes and in D some of HS-anMan stainings that remained in the holes.

Fig 6. Association of ascorbate-induced nuclear HS-anMan with variously acetylated histone H3. Deconvolution immunofluorescence images of near confluent cultures of WT MEFs which were (A) untreated, or (B) treated with 1 mM ascorbate (Asc) for 30 min, followed (C-G) by chase in fresh medium for the indicated periods of time. Staining was performed with mAb anti-HS-anMan (AM, green), anti-histone H3 with N-acetylated N-terminus (N-Ac-H3, red), anti-histone H3 with acetylated Lys-9 (H3K9Ac, red) and anti-histone H3 with dimethylated Lys-9 ($H3K9Me_2$, red). Exposure time was the same in all cases. A blow-up of the merged image in D is shown in E.

Fig 7. HS-anMan spontaneously released from Gpc-1 and transported to the nucleus in growing cells targets nucleolin. Deconvolution immunofluorescence images of growing WT MEFs (A) 3 h, (B) 6 h and (C) 16 h after growth initiation of sparse, growth-arrested cultures. Staining was performed with mAb anti-HS-anMan (AM, green), and anti-nucleolin (NCL, red). Exposure time was the same in all cases.

Fig 8. HS-anMan spontaneously released from Gpc-1 and transported to the nucleus in growing cells associates with nascent RNA. Deconvolution immunofluorescence images of growing WT MEFs (A) 3 h, (B) 6 h and (C) 16 h after growth initiation. Staining was performed with mAb anti-HS-anMan (AM, green) and nascent RNA was visualized by pulse labeling with ethynyl uridine followed by coupling to Alexa Fluor 594 azide (RNA, red). Exposure time was the same in all cases.

Fig 9. Effect of hypoxia-induced nuclear HS-anMan on nucleolin and nascent RNA in Tg2576 MEF cells. Deconvolution immunofluorescence images of near confluent cultures of Tg2576 MEF at (A, C) normoxic conditions or (B, D) after 2 h of hypoxia. Staining was

performed with mAb anti-HS-anMan (AM, green) and anti-nucleolin (NCL, red) and nascent RNA was visualized by pulse labeling with ethynyl uridine followed by coupling to Alexa Fluor 594 azide (RNA, red). Exposure time was the same in all cases.

Fig 10. Effect of hypoxia-induced, nuclear HS-anMan on nucleolin in growing human U87 glioblastoma cells. Deconvolution immunofluorescence images of growing U87 cells at (A) normoxic or (B-D) hypoxic conditions. Staining was performed with mAb anti-HS-anMan (AM, green) and anti-nucleolin (NCL, red). Exposure time was the same in all cases.

Fig 11. Effect of hypoxia-induced, nuclear HS-anMan on nascent RNA in growing human U87 glioblastoma cells. Deconvolution immunofluorescence images of growing U87 cells at (A) normoxic or (B) hypoxic conditions (low and high magnification). Staining was performed with mAb anti-HS-anMan (AM, green) and nascent RNA was visualized by pulse labeling with ethynyl uridine followed by coupling to Alexa Fluor 594 azide (RNA, red). Exposure time was the same in all cases.

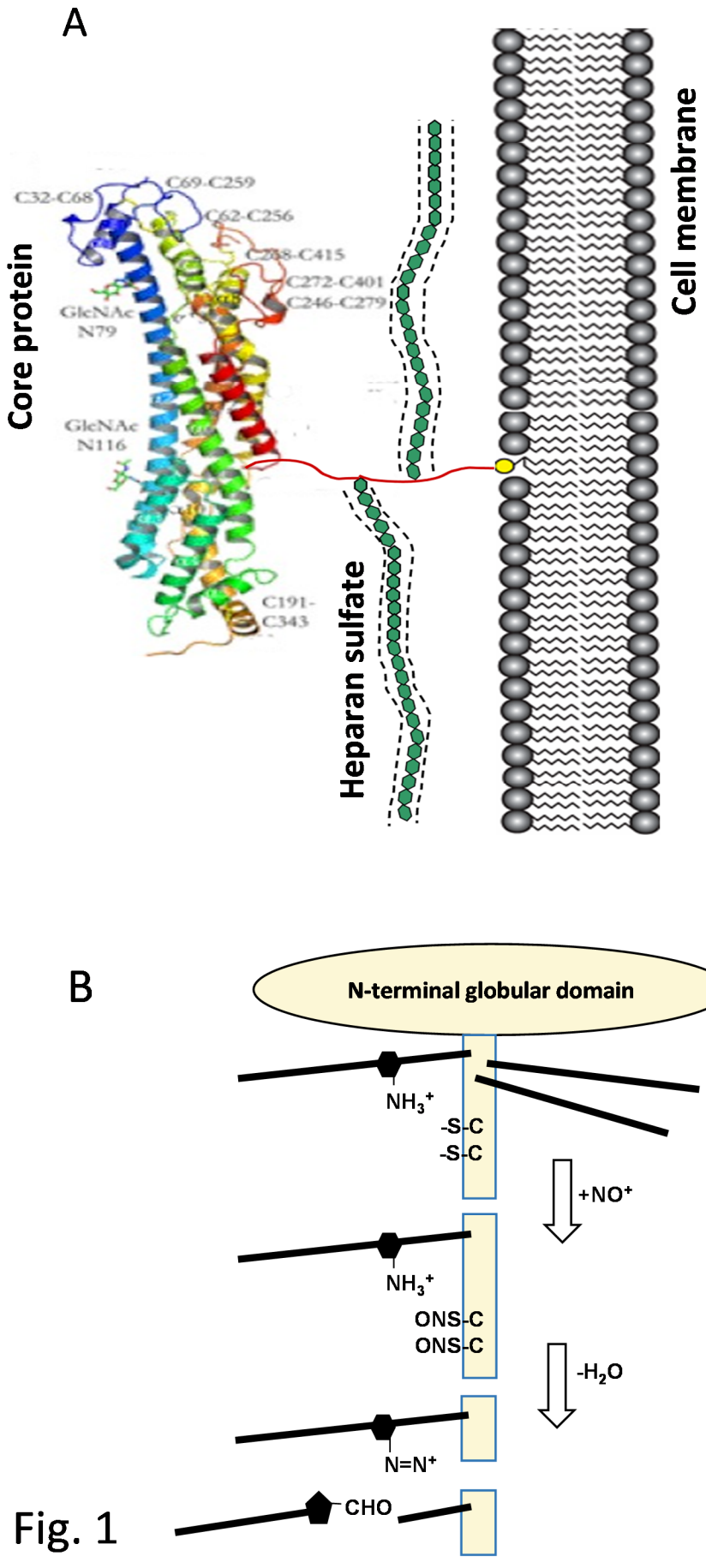
A
Core protein
Cell membrane
Heparan sulfate
C32-C68
C69-C259
C62-C256
C288-C415
C272-C401
C246-C279
GlcNAc
N79
GlcNAc
N116
C191-
C343
B
N-terminal globular domain
NH3+
-S-C
-S-C
+NO+
NH3+
ONS-C
ONS-C
-H2O
N=N+
CHO

Fig. 1

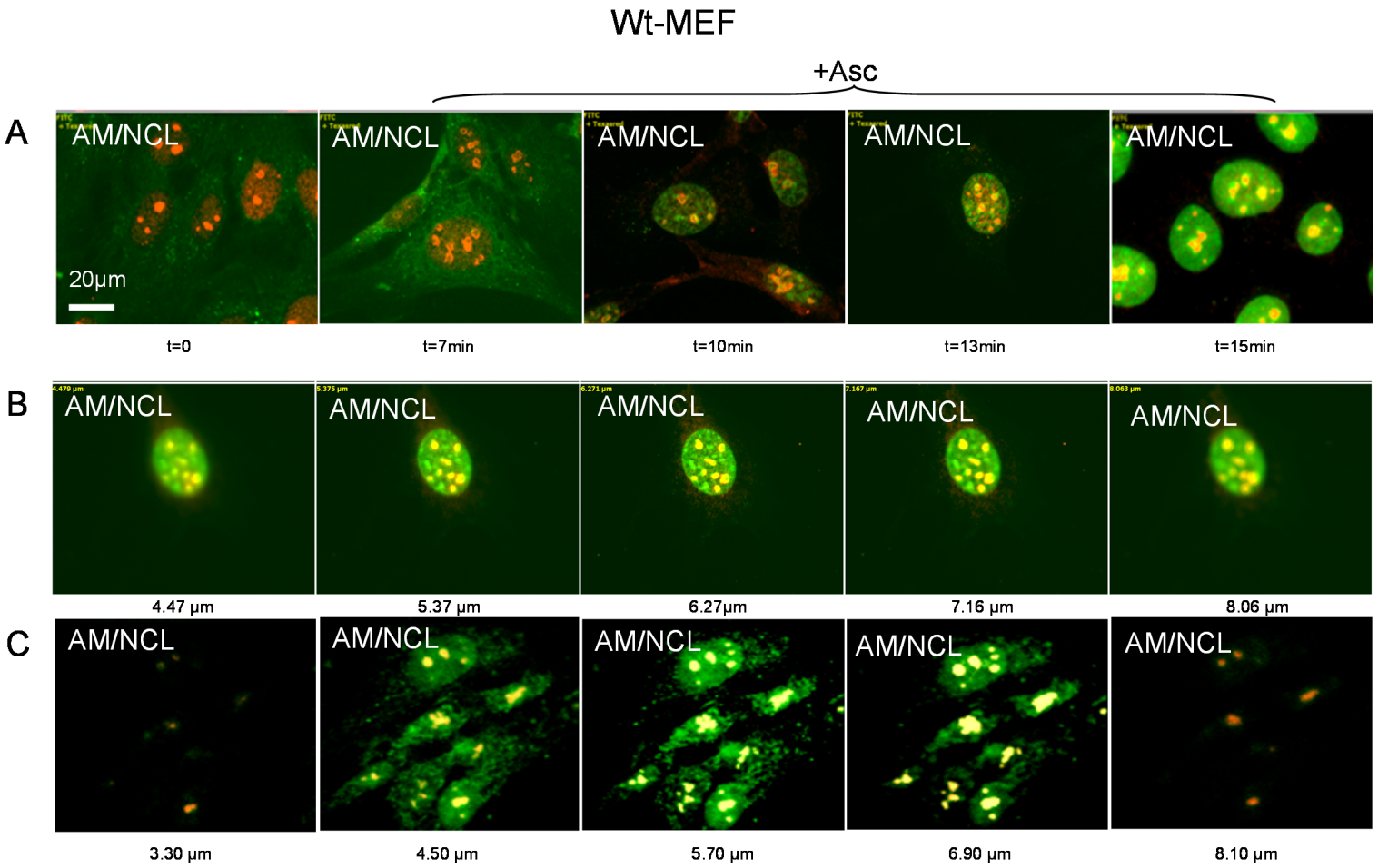
Wt-MEF
+Asc
A
AM/NCL
20µm
t=0
t=7min
t=10min
t=13min
t=15min
B
4.47 µm
5.37 µm
6.27µm
7.16 µm
8.06 µm
C
3.30 µm
4.50 µm
5.70 µm
6.90 µm
8.10 µm

Fig. 2

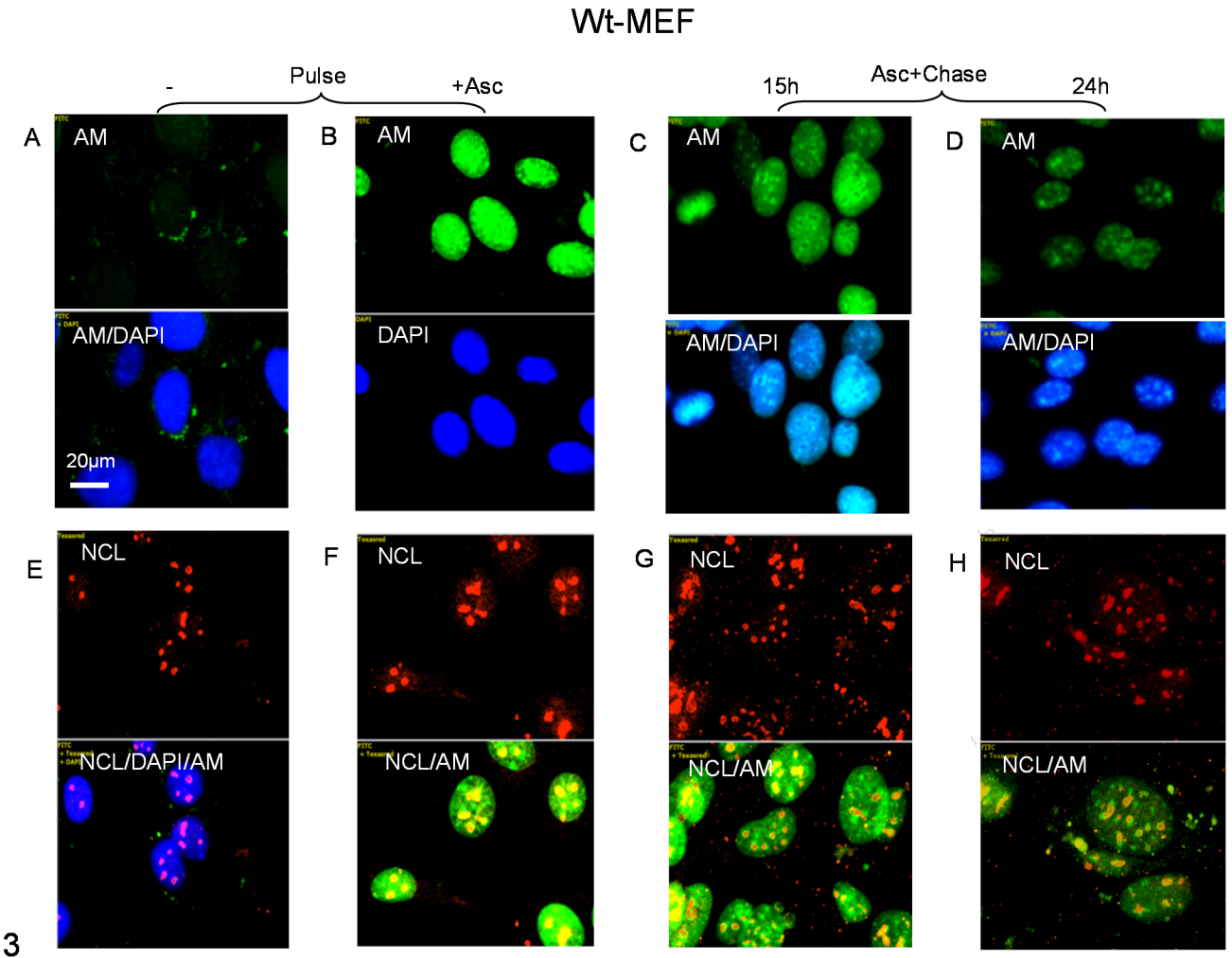
Wt-MEF
-
Pulse
+Asc
15h
Asc+Chase
24h
A
AM
AM/DAPI
20μm
B
AM
DAPI
C
AM
AM/DAPI
D
AM
AM/DAPI
E
NCL
NCL/DAPI/AM
F
NCL
NCL/AM
G
NCL
NCL/AM
H
NCL
NCL/AM

Fig. 3

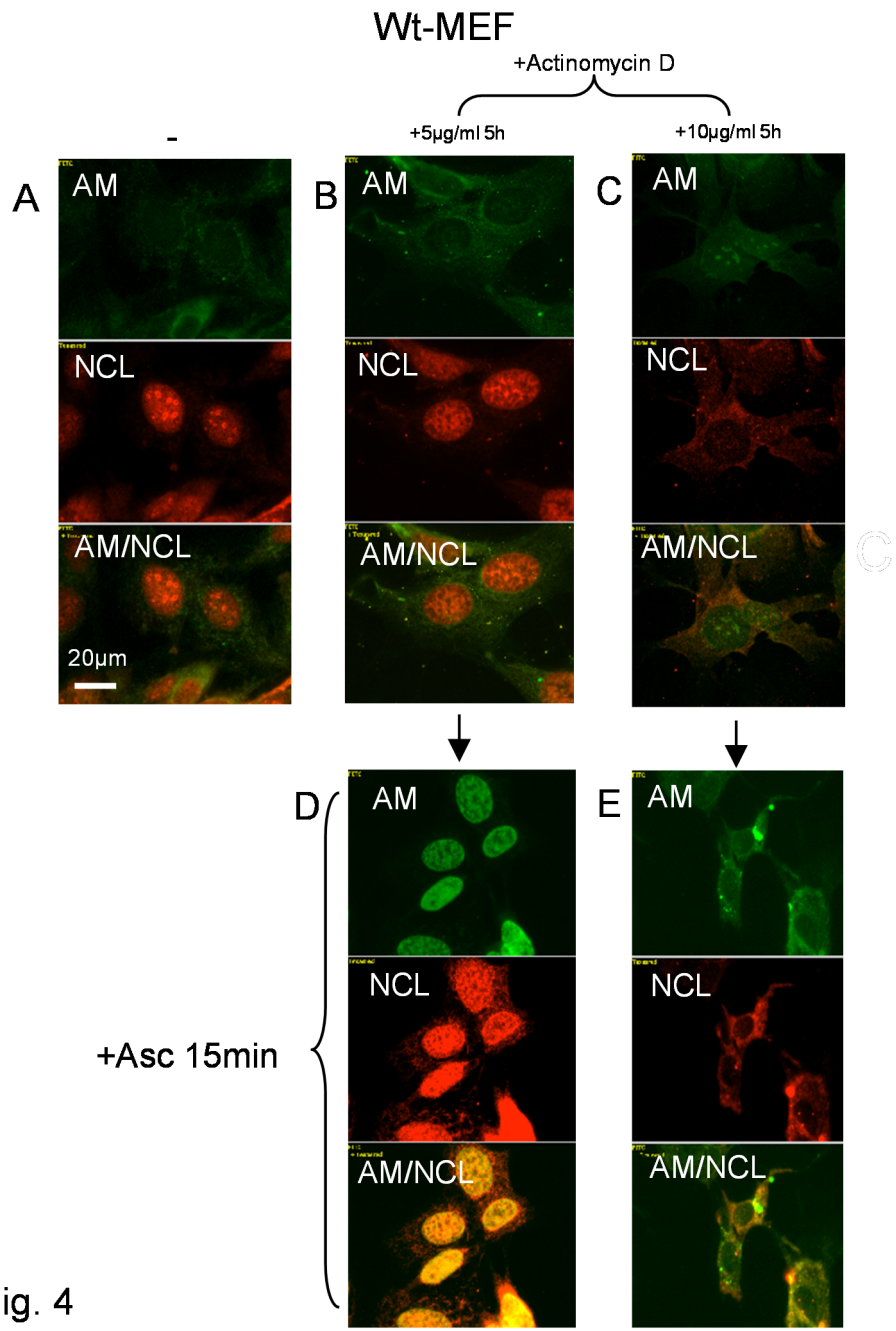
Wt-MEF
+Actinomycin D
-
+5μg/ml 5h
+10μg/ml 5h
A
B
C
AM
NCL
AM/NCL
20μm
D
E
+Asc 15min

Fig. 4

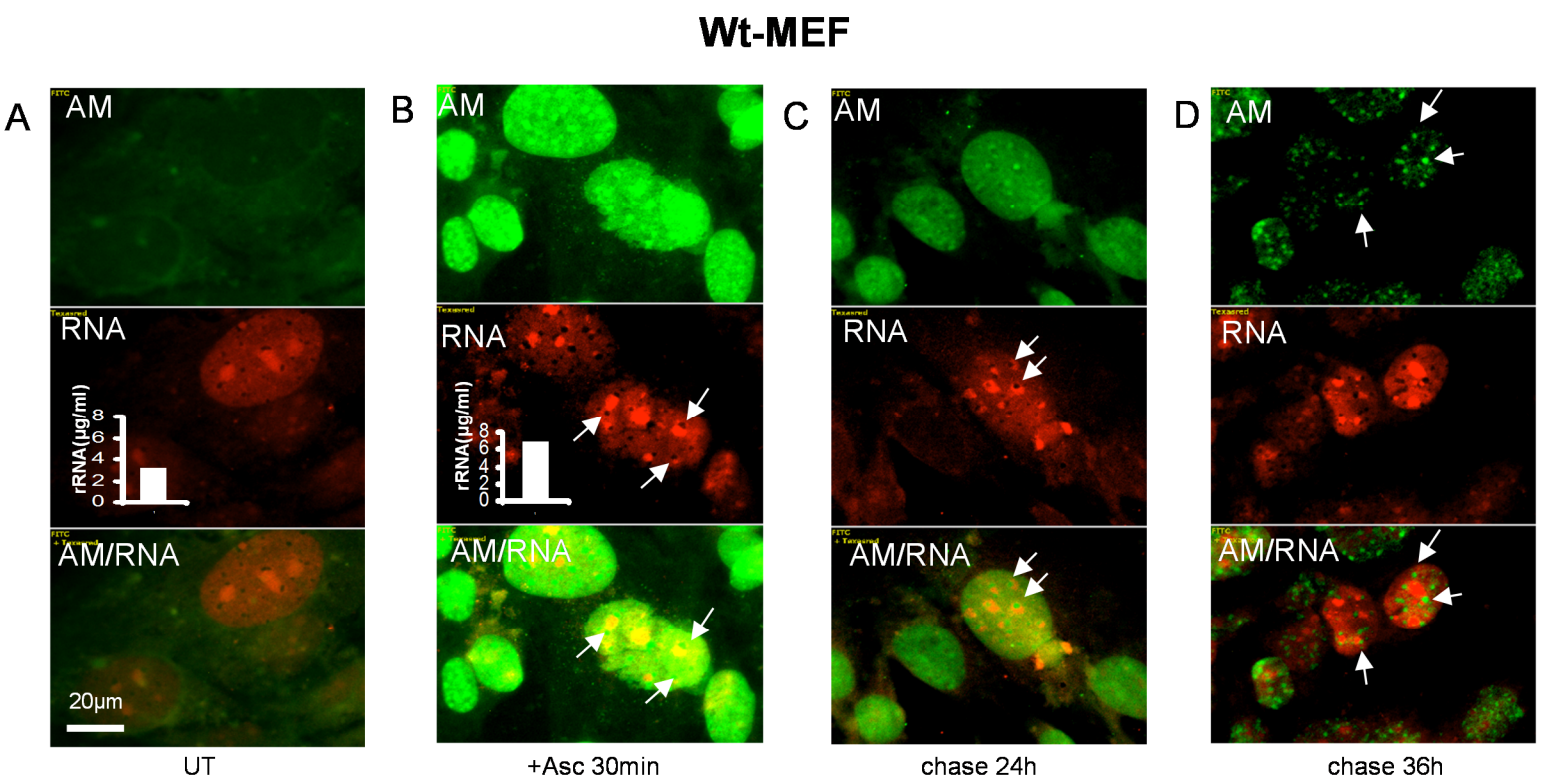
Wt-MEF
A
AM
RNA
rRNA(μg/ml)
8
6
4
2
0
AM/RNA
20μm
B
AM
RNA
rRNA(μg/ml)
8
6
4
2
0
AM/RNA
C
AM
RNA
AM/RNA
D
AM
RNA
AM/RNA
UT
+Asc 30min
chase 24h
chase 36h

Fig. 5

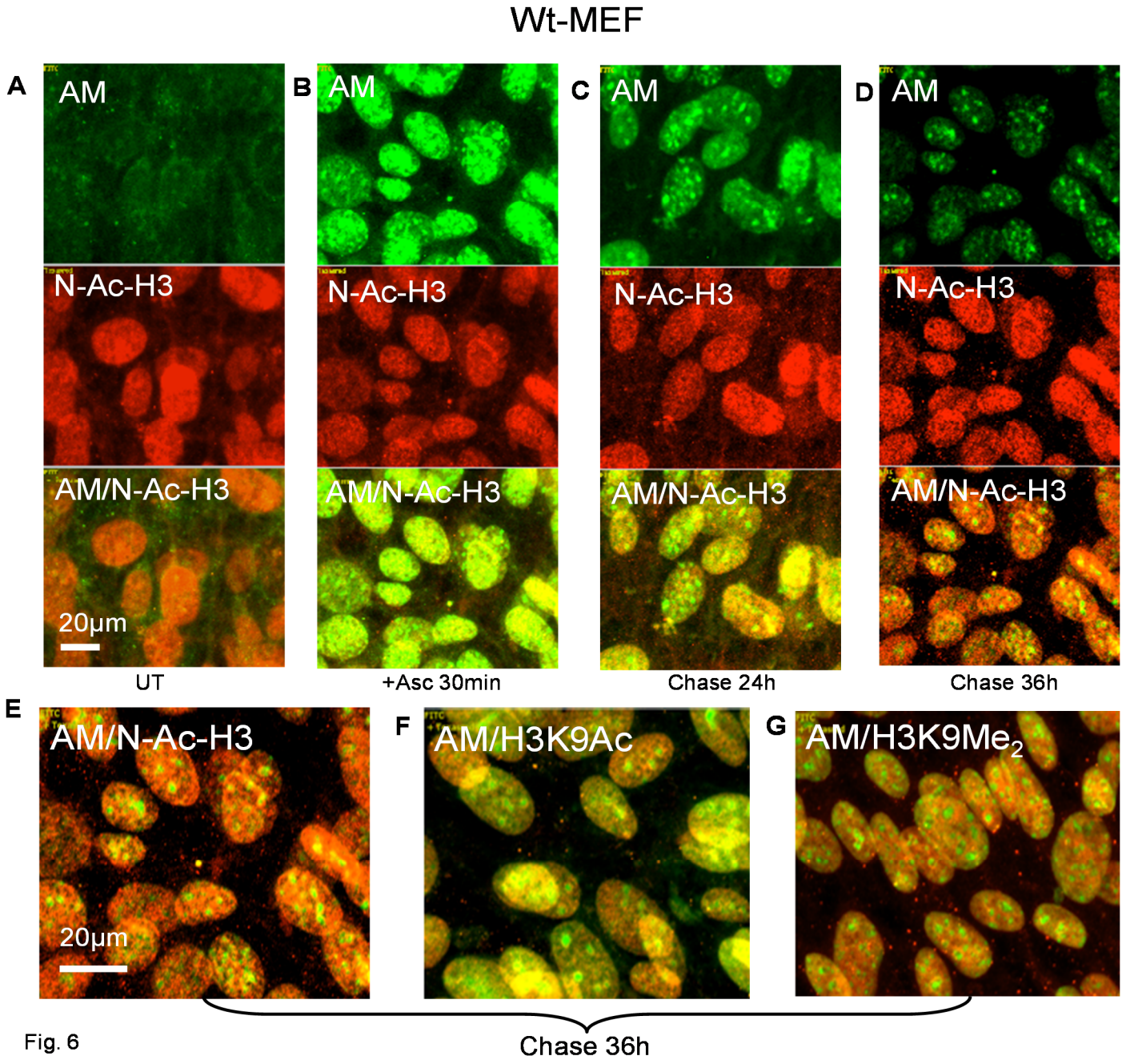
Wt-MEF
A
AM
N-Ac-H3
AM/N-Ac-H3
20μm
UT
B
AM
N-Ac-H3
AM/N-Ac-H3
+Asc 30min
C
AM
N-Ac-H3
AM/N-Ac-H3
Chase 24h
D
AM
N-Ac-H3
AM/N-Ac-H3
Chase 36h
E
AM/N-Ac-H3
20μm
F
AM/H3K9Ac
G
AM/H3K9Me2
Chase 36h

Fig. 6

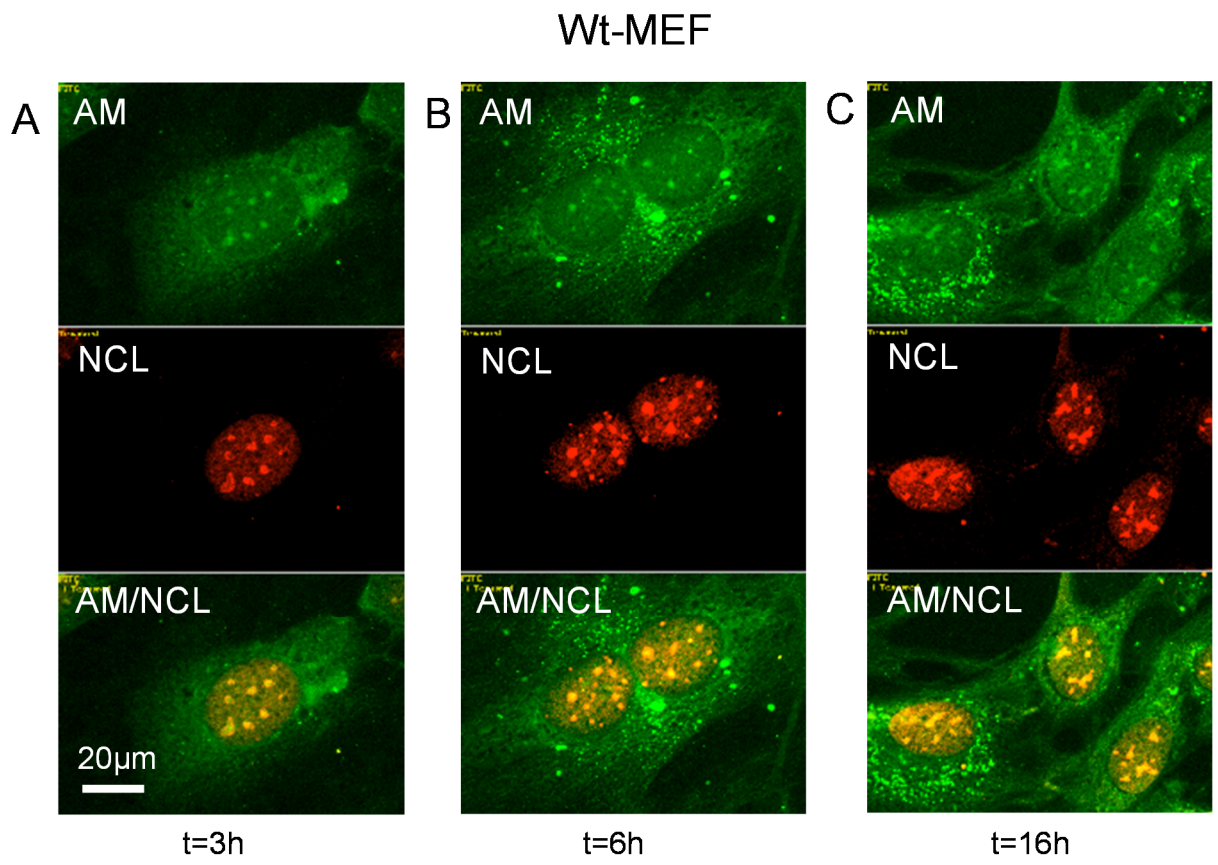
Wt-MEF
A
AM
NCL
AM/NCL
20μm
B
AM
NCL
AM/NCL
C
AM
NCL
AM/NCL
t=3h
t=6h
t=16h

Fig. 7

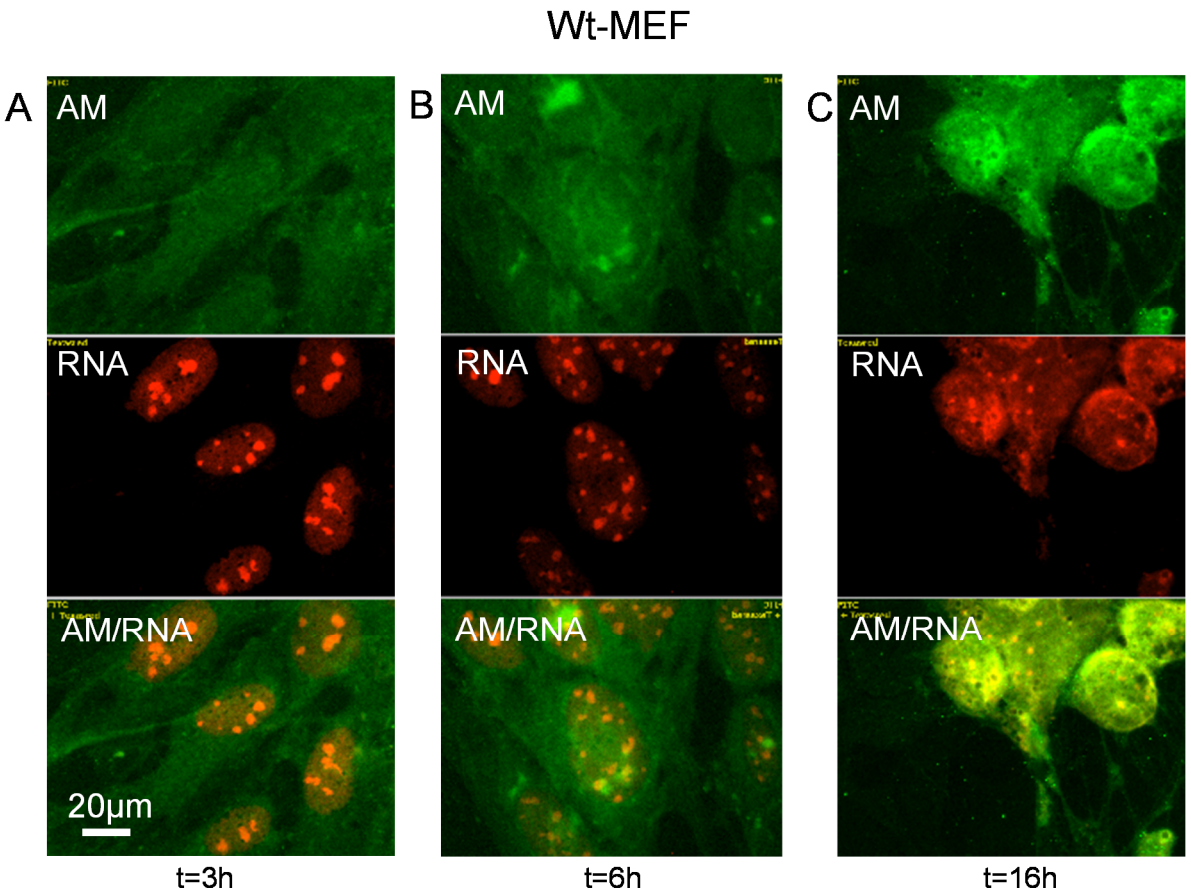
Wt-MEF
A
AM
RNA
AM/RNA
20µm
B
AM
RNA
AM/RNA
C
AM
RNA
AM/RNA
t=3h
t=6h
t=16h

Fig. 8

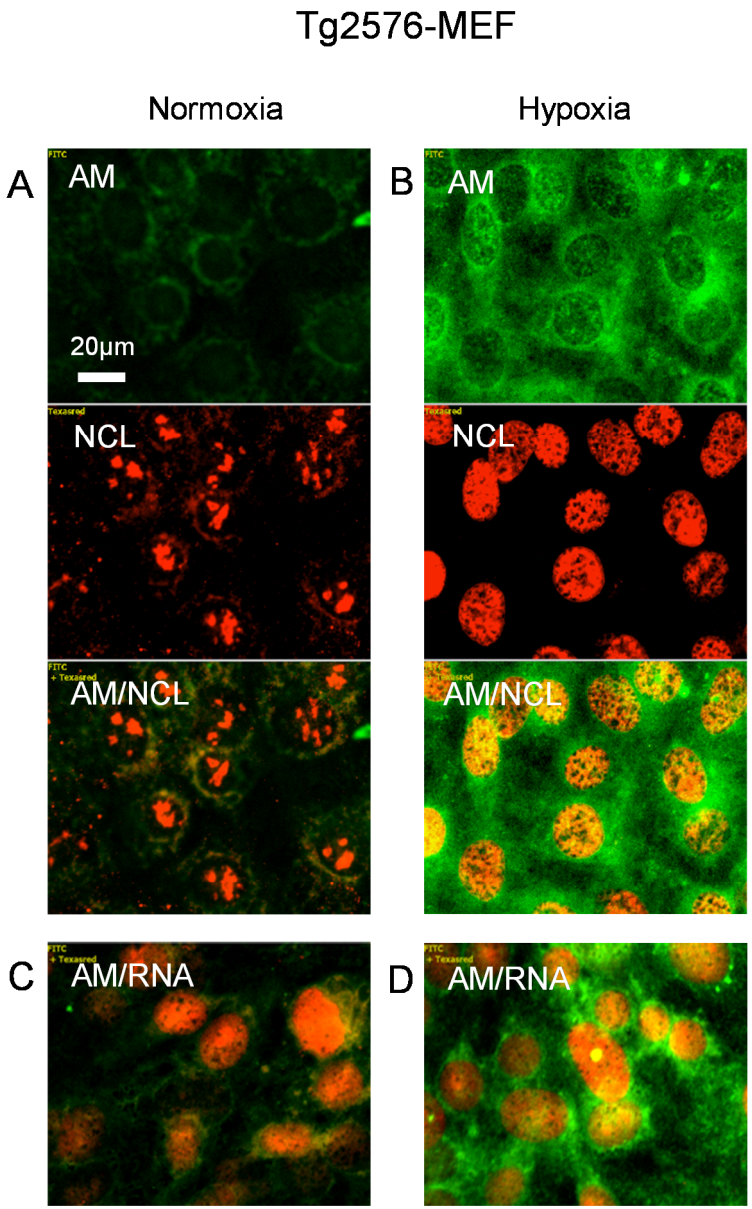
Tg2576-MEF
Normoxia
Hypoxia
A
AM
20μm
NCL
AM/NCL
B
AM
NCL
AM/NCL
C
AM/RNA
D
AM/RNA

Fig. 9

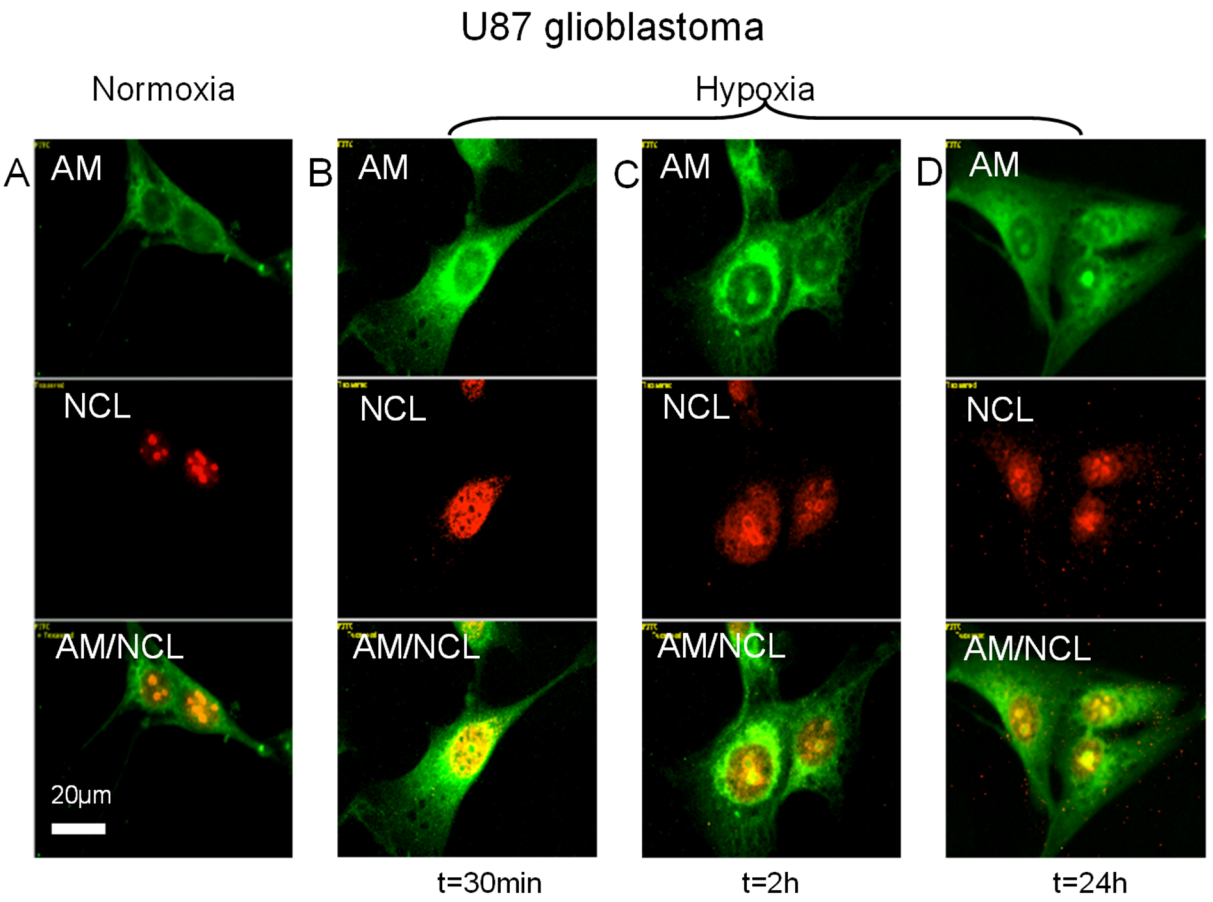
U87 glioblastoma
Normoxia
Hypoxia
A
AM
NCL
AM/NCL
20µm
B
AM
NCL
AM/NCL
C
AM
NCL
AM/NCL
D
AM
NCL
AM/NCL
t=30min
t=2h
t=24h

Fig. 10

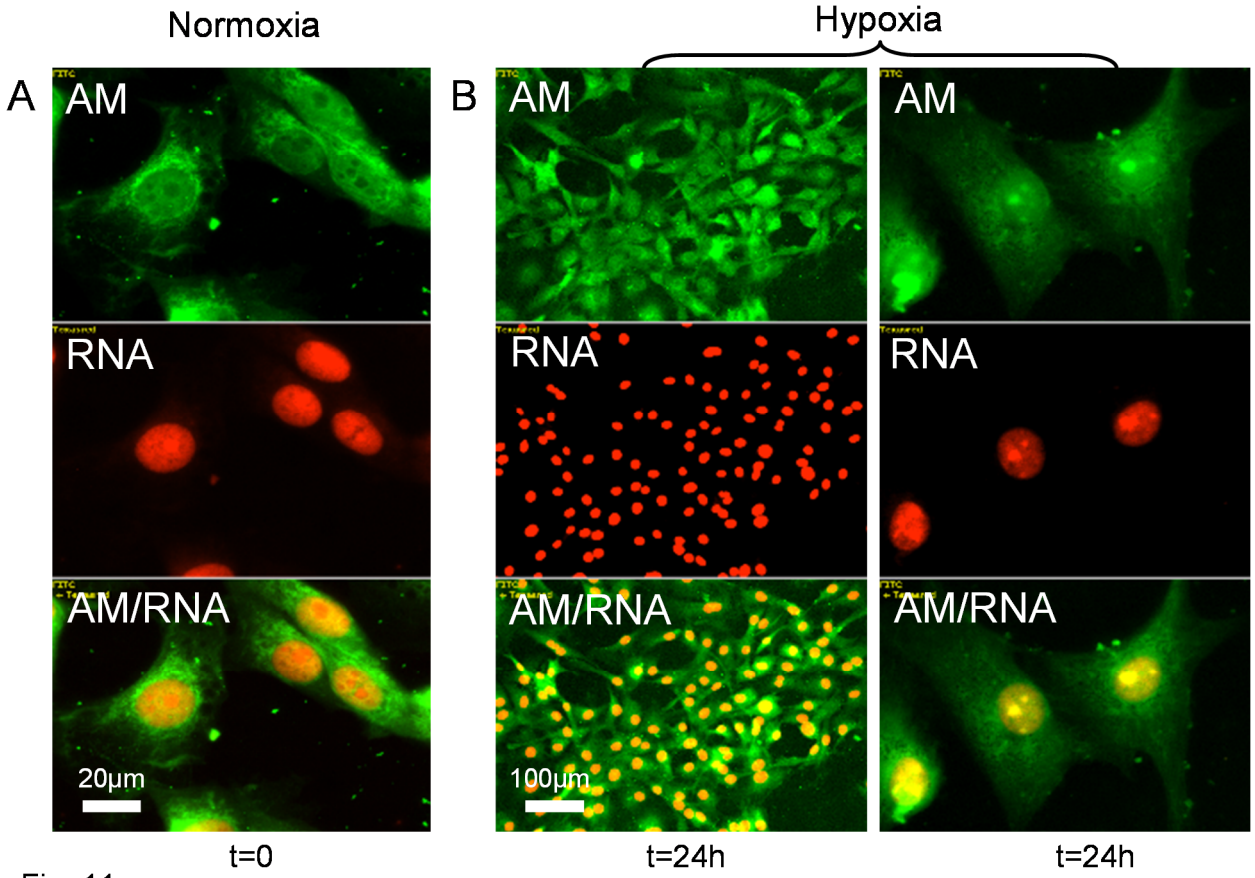
U87 glioblastoma
Normoxia
Hypoxia
A
B
AM
RNA
AM/RNA
AM
RNA
AM/RNA
AM
RNA
AM/RNA
20µm
100µm
t=0
t=24h
t=24h

Fig. 11